

# FTIR Spectroscopy Combined with Isotope Labeling and Quantum Chemical Calculations to Investigate Adsorbed Bicarbonate Formation Following Reaction of Carbon Dioxide with Surface Hydroxyl Groups on Fe<sub>2</sub>O<sub>3</sub> and Al<sub>2</sub>O<sub>3</sub>

Jonas Baltrusaitis, Jan H. Jensen, and Vicki H. Grassian\*

Department of Chemistry, University of Iowa, Iowa City, Iowa 52242

Received: December 21, 2005; In Final Form: February 22, 2006

FTIR spectroscopy combined with isotope labeling experiments and quantum chemical calculations is used to investigate the adsorption of carbon dioxide on hydroxylated metal oxide surfaces. In particular, transmission FTIR spectra following CO<sub>2</sub> adsorption on hydroxylated nanoparticulate Fe<sub>2</sub>O<sub>3</sub>,  $\alpha$ -Al<sub>2</sub>O<sub>3</sub>, and  $\gamma$ -Al<sub>2</sub>O<sub>3</sub> particles at 296 K are reported. As expected, reaction of CO<sub>2</sub> with these surfaces results in the formation of adsorbed bicarbonate and carbonate. In this study, the vibrational spectrum of the bicarbonate product is analyzed in detail through the use of isotope labeling experiments and quantum chemical calculations. The experimental and calculated vibrational frequencies of adsorbed HC<sup>16</sup>O<sub>3</sub><sup>-</sup>, DC<sup>16</sup>O<sub>3</sub><sup>-</sup>, HC<sup>18</sup>O<sub>3</sub><sup>-</sup>, HC<sup>16</sup>O<sup>18</sup>O<sub>2</sub><sup>-</sup>, and HC<sup>18</sup>O<sup>16</sup>O<sub>2</sub><sup>-</sup> indicate that bicarbonate bonds to the surface in a bridged structure. There is some evidence from the mixed isotope experiments that following initial nucleophilic attack of OH, the formation of the final bicarbonate structure involves a proton transfer. On the basis of energetic considerations, the proton transfer mechanism most likely occurs through an intermolecular process involving either coadsorbed hydroxyl groups and/or carbonate.

## Introduction

Surface reactions of carbon dioxide are of great interest for many reasons. In heterogeneous catalysis, carbon dioxide activation is of interest in the industrial production of several important commercial products including methanol and dimethyl carbonate.<sup>1,2</sup> In the environment, carbon dioxide is a prevalent atmospheric gas whose increasing concentration impacts the Earth's climate. As metal oxides are important heterogeneous catalysts,<sup>3,4</sup> and environmental interfaces,<sup>5–8</sup> the interaction of carbon dioxide with oxide surfaces is of interest for a number of different reasons. From an environmental perspective, iron oxides in particular are a common reactive component of air, water, and soil, and the surface chemistry of iron oxides under ambient conditions plays a crucial role in a number of wide ranging environmental processes. For example, Fe-containing minerals such as hematite,  $\alpha$ -Fe<sub>2</sub>O<sub>3</sub>, present in the atmosphere as a component of the mineral dust aerosol, are an important nutrient source for ocean life.<sup>9–11</sup> Surface reactions involving Fe-containing mineral dust aerosol including hematite can increase the amount of bioavailable iron, i.e., Fe(II).<sup>12</sup>

There have been a number of infrared spectroscopy studies of carbon dioxide adsorption on hydroxylated metal oxide surfaces, including iron oxide, and oxide-supported metal catalysts.<sup>13–24</sup> The formation of adsorbed carbonates, bicarbonates, carboxylates, and formates, as well as bent CO<sub>2</sub> species, have been observed. On the basis of the observed infrared absorption band frequencies, vibrational assignments have been made to various surface species. In the case of adsorbed carbonate, the identification of the type of surface structure that forms, i.e., bidentate, monodentate, or bridge, is based on the splitting of the doubly degenerate  $\nu_3$  vibrational mode of the

carbonate ion, since lowering of the symmetry due to adsorption results in the splitting of this degenerate vibration. In a comprehensive compilation of infrared frequencies observed following CO<sub>2</sub> adsorption on oxide surfaces, Busca and Lorenzelli summarize the literature prior to 1982 and propose on the basis of this literature that the splitting  $\Delta\nu_3$  is  $\sim 100$  cm<sup>-1</sup> for monodentate adsorbed carbonate,  $\sim 300$  cm<sup>-1</sup> for bidentate adsorbed carbonate, and 400 cm<sup>-1</sup> or higher for bridged adsorbed carbonate structures.<sup>13</sup> While the assignments of the different structures of adsorbed carbonate have been discussed in the literature in some detail and are briefly summarized above, there has been much less discussion with respect to adsorbed bicarbonate. The focus of this paper is on the structure of adsorbed bicarbonate on oxide surfaces, in particular iron and aluminum oxides.

Bicarbonate ion in the solid state forms a hydrogen-bonded dimer structure as indicated by a shift of the O–H stretch,  $\nu$ -(O–H), from  $\sim 3200$  to  $\sim 2550$  cm<sup>-1</sup>.<sup>26–29</sup> Both bidentate and monodentate bicarbonate bonding has been observed in the case of organometallic monomeric Rh complexes.<sup>30,31</sup> In the review of Busca and Lorenzelli,<sup>13</sup> there was a brief discussion of adsorbed bicarbonate and it was suggested that bicarbonate can adsorb as either monodentate and bidentate structures on the surface. They also discussed the possibility of a bridged bicarbonate structure but indicated there was no evidence of its existence. Rethwisch and Dumesic assigned some of the observed infrared bands of CO/CO<sub>2</sub> mixtures adsorbed on a series of metal oxides to a monodentate bicarbonate structure, M–O–CO<sub>2</sub>H where M is a metal atom.<sup>24</sup> Auroux and Gervasini also proposed that bicarbonate forms a monodentate surface species on metal oxides.<sup>23</sup> Turek et al. propose that bicarbonate forms on several alumina-supported metal oxide catalysts and they indicate that the structure for this surface species is

\* To whom correspondence should be addressed.

monodendate as indicated by,  $\text{M-OH-CO}_2$ .<sup>19</sup> The bond connectivity drawn by Turek et al. differs from that drawn by Arous and Gervasini<sup>23</sup> and Rethwisch and Dumesic.<sup>24</sup> Furthermore, Jung and Bell propose that bicarbonate on zirconia forms a structure they denote as bidendate which is shown as a bridged structure,  $\text{M}_2\text{O}_2\text{COH}$ .<sup>25</sup>

From the above discussion, there seems to be a variety of surface structures assigned to adsorbed bicarbonate. Many of the infrared spectra reported for these various structures are similar if not nearly identical. As a first step in investigating  $\text{CO}_2$  interactions on hydroxylated oxide surfaces under a variety of environmental conditions of temperature and relative humidity, we have combined transmission FTIR spectroscopy, isotope labeling studies and quantum chemical calculations to provide further insights into the molecular structure of the adsorbed products as well as the surface chemistry of  $\text{CO}_2$  with hydroxylated metal oxide particles. The focus of this paper is on the adsorbed bicarbonate product that forms under dry conditions ( $\text{RH} < 1\%$ ) and whose absorption bands often dominate the infrared spectrum when gas-phase  $\text{CO}_2$  is present.

## Experimental Section

**Transmission FTIR Spectroscopy.** FTIR spectroscopy has been used to measure the vibrational spectra of several oxide surfaces in equilibrium with gas-phase  $\text{CO}_2$ . The infrared spectra were collected using a single beam FTIR spectrometer, Mattson Research Series, equipped with a liquid nitrogen cooled narrowband mercury cadmium telluride (MCT) detector. A total of 250 scans were acquired at an instrument resolution of  $4\text{ cm}^{-1}$  over the spectral range from 800 to  $4000\text{ cm}^{-1}$ . The spectrometer was purged with a commercially available air-dryer (Balston 75-62) which minimized  $\text{H}_2\text{O}$  and  $\text{CO}_2$  concentrations in the purge air.

An infrared cell made from a stainless steel cube was placed in the sample compartment of the spectrometer. This infrared cell has been described previously.<sup>32,33</sup> Two  $\text{BaF}_2$  windows (Janos Technology Inc.) were placed into two stainless steel holders, which were sealed by O-rings to the IR cell. Approximately 5–15 mg of oxide powder were pressed onto half of a tungsten grid; the other half was left uncoated and was used to measure the infrared spectrum of the gas phase. The infrared cell was connected to a gas-handling system which consists of a glass manifold with four ports connected to two absolute pressure transducers (MKS instruments) that operate in two different ranges from 0.001 to 10.00 Torr and from 0.1 to 1000 Torr. The gas manifold, connected to a turbo molecular pump, can be used to pump the system down to a final pressure of around  $1 \times 10^{-6}$  Torr. The gas handling system is connected to the IR cell and  $\text{CO}_2$  gas cylinders through a Teflon tube.

The infrared cell sits on a linear translator inside of the internal compartment of the spectrometer so that the position of IR cell can be changed with respect to the infrared beam path. The half of the grid coated with the oxide powder yields spectral features associated with the oxide surface and surface adsorbates as well as gas phase spectral features, whereas the uncoated half of the grid only yields information about the gas phase. Single beam spectra of the oxide powder in the presence of  $\text{CO}_2$  or after exposure to  $\text{CO}_2$  were all referenced to those prior to exposure to give the absorbance spectra of both surface adsorbed and gas phase species. Information about adsorbed surface species only could then be obtained by spectral subtraction of the gas-phase spectrum under identical conditions. All IR spectra were recorded at 296 K.

**Sources of Oxide Powders, Water, and Carbon Dioxide.** Commercially available  $\text{Fe}_2\text{O}_3$  and  $\text{Al}_2\text{O}_3$  powders were used

in these experiments. Nanoparticulate amorphous  $\text{Fe}_2\text{O}_3$  with a surface area of  $229\text{ m}^2\text{ g}^{-1}$  was purchased from Alfa Aesar. Scanning electron microscopy shows 30 nm aggregates composed of smaller particles approximately 2–5 nm in diameter. Mossbauer spectroscopy indicates that the nanoparticulate  $\text{Fe}_2\text{O}_3$  contains hematite and ferrihydrite.  $\alpha\text{-Al}_2\text{O}_3$  with a surface area of  $12.4\text{ m}^2\text{ g}^{-1}$  was also purchased from Alfa Aesar and  $\gamma\text{-Al}_2\text{O}_3$  with a surface area of  $101\text{ m}^2\text{ g}^{-1}$  was purchased from Degussa (AlumOxid C). All surface areas were measured using a Quantachrome Nova 1200 Multipoint BET apparatus.

Water vapor was taken from the headspace above several different liquid samples, depending on the isotope used. Distilled  $\text{H}_2\text{O}$  (Optima grade) was purchased from Fisher Scientific and was degassed prior to use. Deuterium-labeled water,  $\text{D}_2\text{O}$ , was purchased from Aldrich (99.9 atom % D), and  $^{18}\text{O}$ -labeled water,  $\text{H}_2^{18}\text{O}$ , was purchased from ISOTEC (minimum 95 atom %  $^{18}\text{O}$ ). Distilled and deuterium-labeled water were degassed prior to use.  $^{18}\text{O}$ -labeled water was transferred to the flask in the presence of nitrogen atmosphere and was used as received. Carbon dioxide was purchased from Air Products (CP grade).  $^{18}\text{O}$ -labeled carbon dioxide gas,  $\text{C}^{18}\text{O}_2$ , was purchased from ISOTEC (minimum 97 atom %  $^{18}\text{O}$ ).

**Quantum Chemical Calculations.** Quantum chemical calculations for the models discussed below were performed using Spartan '04 for Windows (version 1.0.1) software package.<sup>34</sup> One Pentium IV 2.8 GHz processor with 2 GB of memory was utilized for calculations. The results were visualized using commercially available ChemCraft software.<sup>35</sup>

Quantum chemical calculations were performed on binuclear clusters with bicarbonate ion coordinated in different ways. These binuclear cluster models are of the formula  $[\text{M}_2(\text{OH})_4(\mu\text{-OH})(\text{H}_2\text{O})_x(\text{HCO}_3^-)]$ , where  $\text{M} = \text{Al}$  and  $x = 0$  or 1). The amount of coordinated  $\text{H}_2\text{O}$  was adjusted to maintain 4-fold coordination of the Al atoms and charge neutrality. The geometries of the energy minimized clusters at the B3LYP/6-31+G(d) level of theory are shown in Figure 1.

Both energy optimization and vibrational frequency calculations were performed at the B3LYP hybrid DFT level of theory with a 6-31+G(d) basis set. To account for anharmonicity in the calculated vibrational frequencies, a scaling factor was determined according to the procedure recommended in the National Institute of Standards and Technology (NIST) Computational Chemistry Comparison and Benchmark Database.<sup>36</sup> A scaling factor was determined specifically from the frequencies of the monomeric bicarbonate ion in a KBr matrix.<sup>28</sup> Experimental vibrational frequencies ( $\nu_i$ ) and the calculated vibrational frequencies ( $\omega_i$ ) were used to determine the scaling factor ( $c$ ) according to eq 1:

$$c = \sum(\nu_i \cdot \omega_i) / \sum(\omega_i^2) \quad (1)$$

Several basis sets were examined and results are presented in Table 1. Calculated scaling factor for 6-31+G(d) of 0.9506 is close to the value of 0.9613 determined by Wong<sup>37</sup> who calculated an average scaling factor for a variety of small molecules. Here a value of 0.9506 is used as it is better suited for bicarbonate vibrational frequencies.

In the calculations of the proton-transfer mechanism (vide infra), a larger 6-311+G(d,p) basis set was used that includes both the B3LYP hybrid DFT and MP2 levels of theory in order to optimize cluster geometries, calculate single point energies and to determine transition state geometries. Finally, optimized structures were determined without symmetry constraints on any of the molecules. Stationary points were identified as true minima of the PES (potential energy surface) in all cases because

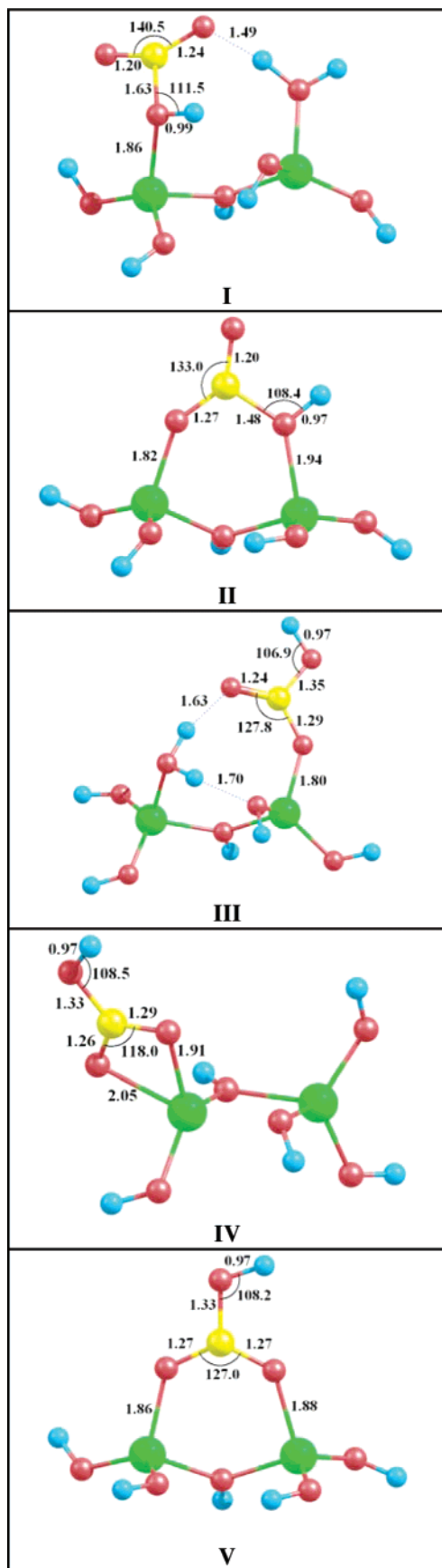


**Figure 1.** Energy minimized structures for five cluster models  $[M_2-(OH)_4(u-OH)(H_2O)_x(HCO_3^-)_z]$  (where  $M = Al$  and  $x = 0$  or  $1$ ) optimized at 6-31+G\* level of theory. Atoms of different elements are highlighted with different colors: metal sites, green; oxygen, red; hydrogen, blue; carbon, yellow.

no imaginary frequencies were found. All transition states (TS) were identified by the presence of one imaginary frequency.

## Results

**Transmission FTIR Spectroscopy of  $CO_2$  Adsorption on Unlabeled Hydroxylated Nanoparticulate  $Fe_2O_3$ ,  $\alpha-Al_2O_3$ , and  $\gamma-Al_2O_3$  Powders Under Dry Conditions at 296 K.** The transmission FTIR spectra of nanoparticulate iron oxide exposed to gas-phase  $CO_2$  as a function of increasing pressure from 51 to 274 mTorr are shown in Figure 2. The final pressure of 274 mTorr is equivalent to atmospheric pressures of  $CO_2$  at the Earth's surface. The most intense bands in the spectra are seen at 1220, 1410, and 1622  $cm^{-1}$ . These bands are characteristic of the formation of adsorbed bicarbonate,  $HCO_3^-$ , and are assigned to the  $\delta_4(COH)$ ,  $\nu_3(OCO)_s$ , and  $\nu_2(OCO)_a$  vibrational modes, respectively. Other bands assigned to bicarbonate are the  $\nu_5(C-OH)$  stretch at 1010  $cm^{-1}$  and the  $\delta_8(CO_2)_{oop}$  band at 820  $cm^{-1}$ . Three remaining bands— $\delta_6(OCO)$ ,  $\nu_9(H$  torsion), and  $\nu_7(OC-(OH))$ —are situated below 800  $cm^{-1}$  region and are not observed due to absorptions of the iron oxide lattice. The higher wavenumber spectral region shown in Figure 2 provides information about surface hydroxyl groups. These OH groups are involved in  $CO_2$  adsorption and bicarbonate formation. The absorption at 3619  $cm^{-1}$  band is due to the O—H stretch in adsorbed bicarbonate. The vibrational assignment of adsorbed bicarbonate product following reaction of  $CO_2$  with surface hydroxyl groups on nanoparticulate iron oxide is given in Table 2.

The broad band near  $\sim 3300$   $cm^{-1}$  can be assigned to hydrogen bonded hydroxyl groups indicate possible hydrogen-bonding interactions between the remaining surface hydroxyl groups and other adsorbates. While it has been shown that the number and position of surface hydroxyl groups depends on iron oxide sample preparation and morphology, hydroxyl groups coordinated to one iron atom is typically found near 3700  $cm^{-1}$  region with more highly coordinated surface hydroxyl groups appearing at lower wavenumbers.<sup>38</sup> Thus, a loss in intensity, as indicated by the negative peaks in the spectra shown in Figure 2, of the O—H groups with frequencies of 3686 and 3664  $cm^{-1}$ , which have been previously assigned to OH groups bonded to two and three metal atoms respectively, show the likely involvement of these specific OH groups in the formation of surface bicarbonate.<sup>38</sup>

Besides the bicarbonate absorption bands, there are several broad overlapping bands observed in the spectral region extending from  $\sim 1100$  to 1600  $cm^{-1}$ ; these bands appear at 1590, 1557, and 1324  $cm^{-1}$  which can be assigned to OCO stretching vibrations of adsorbed carbonates.<sup>13</sup> Absorptions corresponding to symmetric CO stretches for monodentate and bidentate carbonates are observed at 1040 and 1020  $cm^{-1}$ , respectively. The lower frequency region between 800 and 900  $cm^{-1}$  contains absorptions from out-of-plane and in-plane deformation modes of both monodentate and bidentate carbonates.<sup>13</sup>

Transmission FTIR experiments of the nanoparticulate  $Fe_2O_3$  particles following exposure to 274 mTorr of  $CO_2$  as a function of evacuation time were done to provide insight into the stability of adsorbed bicarbonate and carbonate on nanoparticulate  $Fe_2O_3$  surfaces. Adsorbed bicarbonate was found to be unstable with respect to evacuation of gas-phase  $CO_2$ . As seen in Figure 3a, adsorbed bicarbonate bands at 1220, 1410, and 1622  $cm^{-1}$  decrease significantly in intensity upon evacuation at room temperature and almost completely disappear after 120 min. Upon evacuation (see Figure 3b), the bands that remain in the spectrum are due to adsorbed carbonates which are assigned to



**TABLE 1: Scaling Factors Determined for Gas-Phase Bicarbonate Ion at DFT/B3LYP Level of Theory<sup>a</sup>**

vibrational mode	experimental frequency (cm <sup>-1</sup> ) <sup>b</sup>	calculated frequency (cm <sup>-1</sup> ) for the basis set					
		6-31G(d)	6-31G(d,p)	6-31+G(d)	6-311G(d)	6-311+G(d,p)	6-31G(2df,p)
$\nu_1(\text{OH})$	3390	3725	3790	3738	3764	3818	3799
$\nu_2(\text{OCO})_a$	1697	1846	1844	1770	1823	1765	1832
$\nu_3(\text{OCO})_s$	1338	1333	1333	1301	1312	1290	1323
$\delta_4(\text{COH})$	1211	1206	1195	1206	1220	1202	1195
$\nu_5(\text{C—OH})$	960	876	877	853	859	838	870
$\delta_6(\text{OCO})$	712	623	623	619	622	619	628
$\nu_7(\text{OC—(OH)})$	579	537	536	524	549	543	540
$\delta_8(\text{CO}_2)_{\text{oop}}$	835	807	807	805	824	814	824
$\nu_9(\text{H torsion})$	660	570	563	556	582	548	567
scaling factor <sup>c</sup>		0.9440	0.9345	0.9506	0.9395	0.9385	0.9339

<sup>a</sup> Geometry optimization performed at the same basis set before vibrational analysis. <sup>b</sup> From ref 28. <sup>c</sup> Scaling factors of calculated frequencies compared to experimental ones were determined using the recommended procedure from NIST;<sup>36</sup> see text for further details.

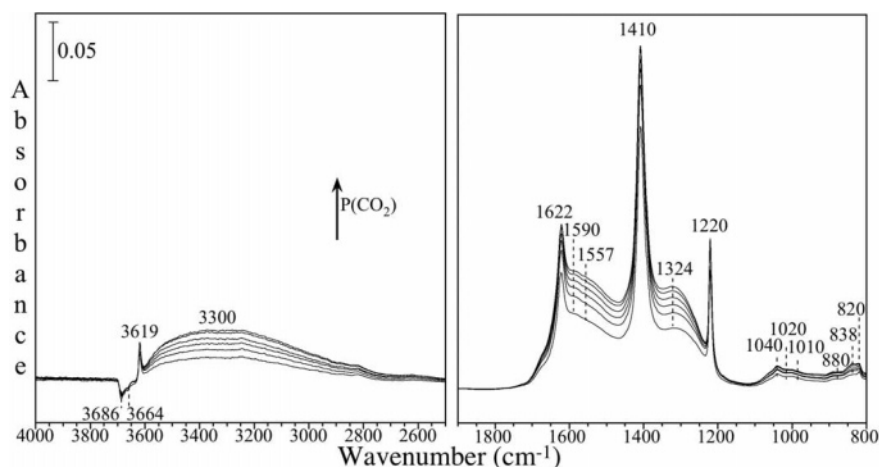


**Figure 2.** Transmission FTIR spectra recorded of nanoparticulate  $\text{Fe}_2\text{O}_3$  following exposure to increasing pressures of  $\text{CO}_2$  (51, 110, 156, 201, 251, and 274 mTorr). All spectra were recorded in the presence of gas-phase  $\text{CO}_2$ .

**TABLE 2: Vibrational Mode Assignment of Adsorbed Bicarbonate Product Following Adsorption of  $\text{CO}_2$  on Hydroxylated Nano- $\text{Fe}_2\text{O}_3$ ,  $\alpha\text{-Al}_2\text{O}_3$ , and  $\gamma\text{-Al}_2\text{O}_3$** 

vibrational mode	frequency (cm <sup>-1</sup> )			
	nano- $\text{Fe}_2\text{O}_3$	$\alpha\text{-Al}_2\text{O}_3$	$\gamma\text{-Al}_2\text{O}_3$	$\text{Al}_2\text{O}_3$ (av value) <sup>a</sup>
$\nu_1(\text{OH})$	3619	n.o. <sup>c</sup>	3623	3623
$\nu_2(\text{OCO})^a$	1622	1650	1648	1649
$\nu_3(\text{OCO})_s$	1410	1433	1438	1435
$\delta_4(\text{COH})$	1220	1230	1231	1231
$\nu_5(\text{C—OH})$	1010	n.o.	n.o.	
$\delta_8(\text{CO}_2)_{\text{oop}}$	820	n.o.	n.o.	

<sup>a</sup> Average value determined from frequencies found for  $\alpha\text{-Al}_2\text{O}_3$  and  $\gamma\text{-Al}_2\text{O}_3$ . For  $\nu_1(\text{OH})$ , this is the value found for  $\gamma\text{-Al}_2\text{O}_3$ . <sup>b</sup> Range taken from refs 13, 16, 19, and 40. <sup>c</sup> n.o. = not observed.

monodentate adsorption (1383 and 1446 cm<sup>-1</sup>) and bidentate adsorption (1316 and 1553 cm<sup>-1</sup>). These peaks have been deconvoluted using a Gaussian curve fit. The peak positions of adsorbed carbonate are found to shift slightly to lower wavenumbers in the absence of gas-phase  $\text{CO}_2$  (Figure 3) compared to in the presence of gas-phase  $\text{CO}_2$  (Figure 2). In addition, the band at 1590 cm<sup>-1</sup>, which is apparent in Figure 1 and assigned to another, less stable form of adsorbed bidentate carbonate, disappear from the spectrum upon evacuation. These observations are consistent with what has been previously observed.<sup>39</sup>

Several additional experiments were done to investigate the vibrational frequencies of adsorbed bicarbonate on  $\alpha\text{-Al}_2\text{O}_3$  and  $\gamma\text{-Al}_2\text{O}_3$  surfaces. The spectra for  $\text{CO}_2$  adsorption on these two surfaces are shown in Figure 4 at a  $\text{CO}_2$  pressure of 274 mTorr along with that for nanoparticulate  $\text{Fe}_2\text{O}_3$ . It can be seen that

the frequencies of the absorption bands of adsorbed bicarbonate are very similar for both phases of aluminum oxides as they only differ by a few wavenumbers. Vibrational frequencies for adsorbed bicarbonate are found to be very close to those on nanoparticulate  $\text{Fe}_2\text{O}_3$ , as shown in Table 2. The vibrational frequencies of adsorbed bicarbonate appear at the same regions for all three metal oxides with observed frequency splittings between  $\nu_3(\text{OCO})_s$  and  $\nu_2(\text{OCO})_a$  of 212, 217, and 210 cm<sup>-1</sup> for nanoparticulate  $\text{Fe}_2\text{O}_3$ ,  $\alpha\text{-Al}_2\text{O}_3$ , and  $\gamma\text{-Al}_2\text{O}_3$ , respectively, thus implying the same structure of adsorbed bicarbonate on all three surfaces. The largest discrepancy between the frequencies found for the aluminum oxide samples and nanoparticulate  $\text{Fe}_2\text{O}_3$  was 28 cm<sup>-1</sup> for both  $\nu_3(\text{OCO})_s$  and  $\nu_2(\text{OCO})_a$ . Thus, the similarities found between the bicarbonate vibrational frequencies for  $\text{Fe}_2\text{O}_3$  and  $\text{Al}_2\text{O}_3$  particle surfaces indicate that similar bicarbonate structures form on both oxides and that the aluminum cluster models used in the quantum chemical calculations will be useful models for these two oxides.

**Transmission FTIR Spectroscopy Coupled With Isotope Labeling Experiments.** Isotope labeling experiments can provide important information on the nature of adsorbed bicarbonate. As will be discussed in detail in the next section, isotope labeling experiments coupled with quantum chemical calculations are particularly useful in determining the structure of the bicarbonate product and providing insights into the mechanism for its formation.

Five different infrared spectra seen in the spectral region extending from 1100 to 2100 cm<sup>-1</sup> are shown in Figure 5. Each spectrum represents a different bicarbonate isotope. Shifts in vibrational frequencies for the characteristic bicarbonate bands—

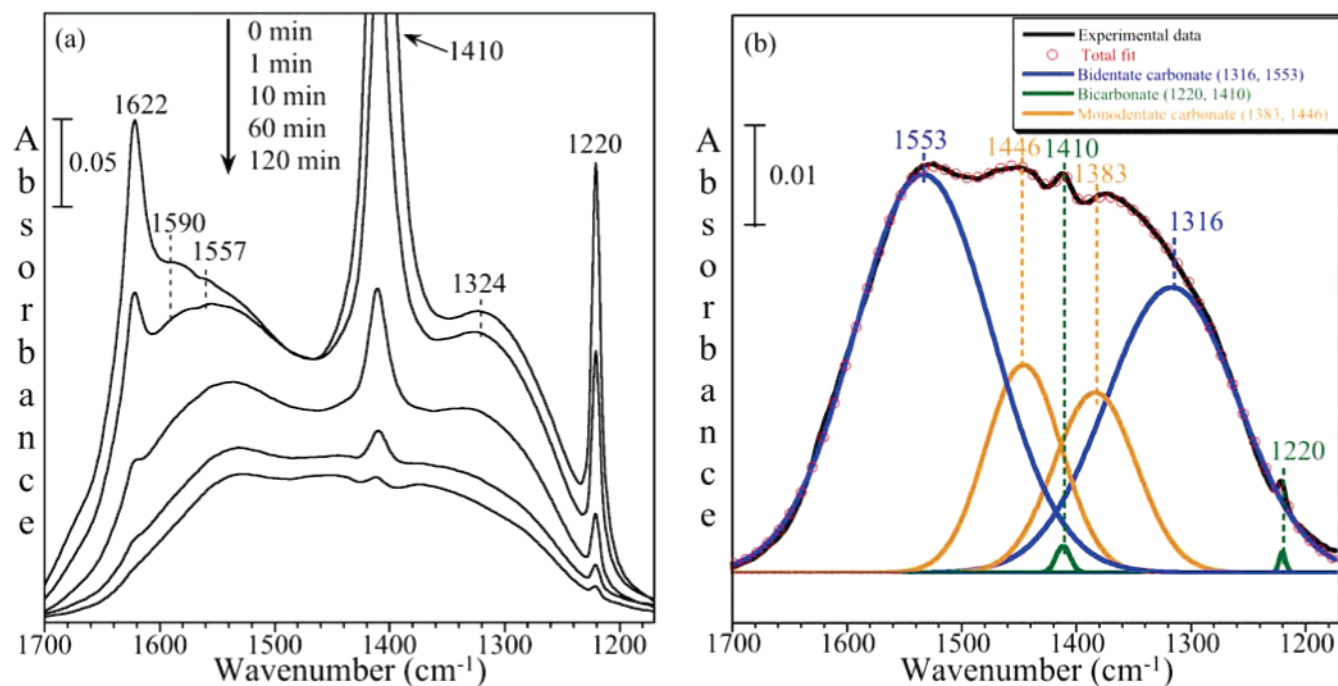


**Figure 3.** Transmission FTIR spectra recorded of nanoparticulate  $\text{Fe}_2\text{O}_3$  particles following exposure to 274 mTorr of  $\text{CO}_2$  as a function of evacuation time from 0 to 120 min (0, 1, 10, 60, and 120 min). (b) Gaussian curve fit for the transmission FTIR spectrum of nanoparticulate  $\text{Fe}_2\text{O}_3$  recorded after exposure of nanoparticulate  $\text{Fe}_2\text{O}_3$  to 274 mTorr of  $\text{CO}_2$  and evacuated for 120 min. The data are fit to three surface species – monodentate carbonate (1383 and 1446  $\text{cm}^{-1}$ ), bidentate carbonate (1316 and 1553  $\text{cm}^{-1}$ ), and bicarbonate (1221 and 1411  $\text{cm}^{-1}$ ). The correlation coefficient for the total fit is 0.99964.

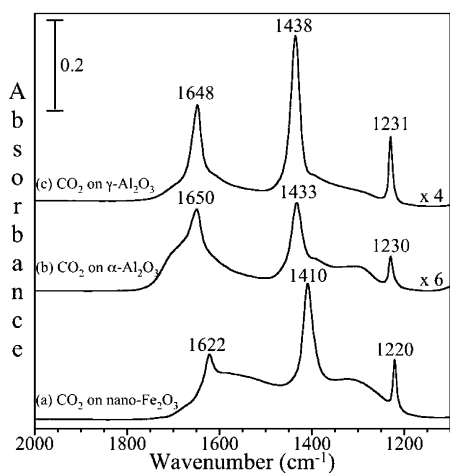


**Figure 4.** Transmission FTIR spectra recorded in the presence of gas-phase  $\text{CO}_2$  at a pressure of 274 mTorr; (a) nanoparticulate  $\text{Fe}_2\text{O}_3$ , (b)  $\alpha\text{-Al}_2\text{O}_3$ , and (c)  $\gamma\text{-Al}_2\text{O}_3$ .

$\delta_4(\text{COH})$ ,  $\nu_3(\text{OCO})_s$ , and  $\nu_2(\text{OCO})_a$ —are observed in the spectra for the different isotopes. In all of these experiments, the  $\text{CO}_2$  pressure is constant at 274 mTorr. The data shown in Figure 5 are for nanoparticulate  $\text{Fe}_2\text{O}_3$ . The bottom spectrum labeled a is the same spectrum shown in Figure 2 in that it is for the adsorption of  $\text{C}^{16}\text{O}_2$  adsorbed on  $^{16}\text{O}$ -labeled hydroxylated  $\text{Fe}_2\text{O}_3$  to yield the bicarbonate product,  $\text{HC}^{16}\text{O}_3^-$ . The spectrum shown in Figure 5b is for  $\text{C}^{16}\text{O}_2$  adsorbed on the iron oxide surface with surface hydroxyl groups that had been exchanged with  $\text{D}_2\text{O}$  to yield  $\text{O}-\text{D}$  groups on the surface.<sup>41</sup> In this experiment, the expected adsorbed bicarbonate product,  $\text{DC}^{16}\text{O}_3^-$ , is formed and most obvious is the shift in frequency of the  $\delta_4(\text{COD})$  from 1220 to 969  $\text{cm}^{-1}$  as we have been reported previously (ref 42) and is not shown here. The small peak at 1220  $\text{cm}^{-1}$  observed in the spectrum is due to  $\text{CO}_2$  reaction with a small amount of residual  $^{16}\text{OH}$  groups that remain on surface after deuteration.

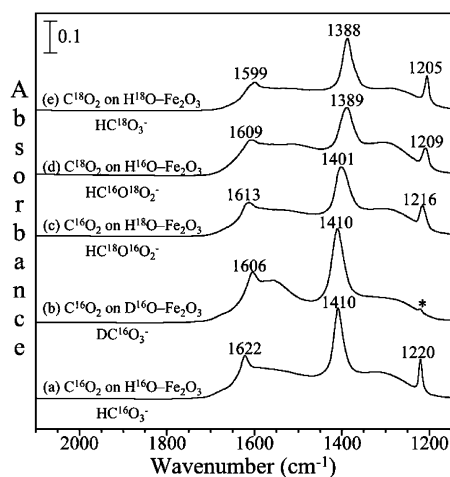


**Figure 5.** Transmission spectra recorded following: (a) 274 mTorr of  $\text{C}^{16}\text{O}_2$  adsorption on nanoparticulate  $\text{Fe}_2\text{O}_3$  with surface  $^{16}\text{OH}$  groups; (b) 274 mTorr of  $\text{CO}_2$  adsorption on nanoparticulate  $\text{Fe}_2\text{O}_3$  with surface  $\text{OD}$  groups; (c) 274 mTorr of  $\text{C}^{16}\text{O}_2$  adsorption on nanoparticulate  $\text{Fe}_2\text{O}_3$  with surface  $\text{O}^{18}\text{H}$  groups present on the surface; (d) 274 mTorr of  $\text{C}^{18}\text{O}_2$  adsorption on nanoparticulate  $\text{Fe}_2\text{O}_3$  with surface  $\text{O}^{16}\text{H}$  groups present on the surface; (e) 274 mTorr of  $\text{C}^{18}\text{O}_2$  adsorption on nanoparticulate  $\text{Fe}_2\text{O}_3$  with surface  $^{18}\text{OH}$  groups present on the surface. Shifts in the frequencies of the absorption bands are seen corresponding to different bicarbonate isotopes ( $\text{HC}^{16}\text{O}_3^-$ ,  $\text{DC}^{16}\text{O}_3^-$ ,  $\text{HC}^{18}\text{O}^{16}\text{O}_2^-$ ,  $\text{HC}^{16}\text{O}^{18}\text{O}_2^-$  and  $\text{HC}^{18}\text{O}_3^-$ ). The asterisk in b indicates the absorption band due to  $\text{CO}_2$  reaction with residual  $-\text{OH}$  surface groups;  $\delta_4(\text{COD})$  is observed at 969  $\text{cm}^{-1}$  (not shown here, but shown in ref 36).

The spectrum shown in Figure 5c was recorded following  $\text{C}^{16}\text{O}_2$  adsorption on an iron oxide surface with surface hydroxyl groups that had been exchanged with  $\text{H}_2^{18}\text{O}$  to yield  $^{18}\text{O}-\text{H}$  groups on the surface. In this experiment, the expected adsorbed bicarbonate product is  $\text{HC}^{18}\text{O}^{16}\text{O}_2^-$ . As can be seen from the infrared spectrum, there are shifts seen in the absorption band frequencies for this partially  $^{18}\text{O}$ -labeled product. The final two spectra

**TABLE 3: Vibrational Frequencies for Different Isotopes of Adsorbed Bicarbonate Following CO<sub>2</sub> Adsorption on Hydroxylated Nano-Fe<sub>2</sub>O<sub>3</sub> and  $\gamma$ -Al<sub>2</sub>O<sub>3</sub>**

oxide	bicarbonate Isotope	vibrational mode and experimental frequency, $\nu$ , (cm <sup>-1</sup> )				vibrational mode and experimental isotope shift, $\Delta\nu_{\text{iso}}^a$			
		$\nu_1(\text{OH})$	$\nu_2(\text{OCO})$	$\nu_3(\text{OCO})_s$	$\delta_4(\text{COH})$	$\nu_1(\text{OH})$	$\nu_2(\text{OCO})_a$	$\nu_3(\text{OCO})_s$	$\delta_4(\text{COH})$
nano-Fe <sub>2</sub> O <sub>3</sub>	HC <sup>16</sup> O <sub>3</sub> <sup>-</sup> ( <sup>16</sup> OH + C <sup>16</sup> O <sub>2</sub> )	3619	1622	1410	1220	0	0	0	0
nano-Fe <sub>2</sub> O <sub>3</sub>	DC <sup>16</sup> O <sub>3</sub> <sup>-</sup> ( <sup>16</sup> OD + C <sup>16</sup> O <sub>2</sub> )	2671	1606	1410	969	-948	-16	0	-251
nano-Fe <sub>2</sub> O <sub>3</sub>	HC <sup>18</sup> O <sub>3</sub> <sup>-</sup> ( <sup>18</sup> OH + C <sup>18</sup> O <sub>2</sub> )	3609	1599	1388	1205	-10	-23	-22	-15
nano-Fe <sub>2</sub> O <sub>3</sub>	HC <sup>18</sup> O <sup>16</sup> O <sub>2</sub> <sup>-</sup> ( <sup>18</sup> OH + C <sup>16</sup> O <sub>2</sub> )	3610	1613	1401	1216	-9	-9	-9	-4
nano-Fe <sub>2</sub> O <sub>3</sub>	HC <sup>16</sup> O <sup>18</sup> O <sub>2</sub> <sup>-</sup> ( <sup>16</sup> OH + C <sup>18</sup> O <sub>2</sub> )	3609	1609	1389	1209	-10	-13	-21	-11
$\gamma$ -Al <sub>2</sub> O <sub>3</sub>	HC <sup>16</sup> O <sub>3</sub> <sup>-</sup> ( <sup>16</sup> OH + C <sup>16</sup> O <sub>2</sub> )	3623	1648	1438	1231	0	0	0	0
$\gamma$ -Al <sub>2</sub> O <sub>3</sub>	HC <sup>16</sup> O <sup>18</sup> O <sub>2</sub> <sup>-</sup> ( <sup>16</sup> OH + C <sup>18</sup> O <sub>2</sub> )	3614	1634	1416	1215	-9	-14	-22	-16

<sup>a</sup>  $\Delta\nu_{\text{iso}} = [\text{isotope labeled frequency} - \text{HC}^{16}\text{O}_3^- \text{ frequency}]$ .

shown in Figures 5d and 5e are recorded following C<sup>18</sup>O<sub>2</sub> adsorbed on a surface with <sup>16</sup>OH and <sup>18</sup>OH groups, respectively. The expected adsorbed bicarbonate product for the experiments shown in parts d and e are HC<sup>16</sup>O<sup>18</sup>O<sub>2</sub><sup>-</sup> and HC<sup>18</sup>O<sub>3</sub><sup>-</sup>, respectively. Shifts in the absorption band frequencies are observed in these isotope experiments as well.

A summary of the vibrational frequencies for each of the five isotopes on nanoparticulate Fe<sub>2</sub>O<sub>3</sub> is given in Table 3. In addition to the absorption bands shown in Figure 5, the  $\nu_1(\text{OH})$  stretching frequency is also given. An additional experiment involving isotope labels was done on  $\gamma$ -Al<sub>2</sub>O<sub>3</sub> and the data from that experiment along with the data from the unlabeled experiment on  $\gamma$ -Al<sub>2</sub>O<sub>3</sub> are also included in Table 3. Besides the absorption band frequencies, the experimentally observed isotope shifts between the labeled bicarbonates and the unlabeled bicarbonate (HC<sup>16</sup>O<sub>3</sub><sup>-</sup>),  $\Delta\nu_{\text{iso}}$ , are tabulated. As discussed below, the experimental vibrational frequencies for these five isotope experiments and the observed shifts are compared to calculated values for several cluster models to better understand the nature of the bonding of adsorbed bicarbonate and the mechanism for the reaction between surface hydroxyl groups and carbon dioxide.

**Quantum Chemical Calculations of Bicarbonate Cluster Models.** Quantum chemical calculations were performed at the B3LYP level of theory with a 6-31+G(d) basis set to elucidate the structure of adsorbed bicarbonate. Vibrational frequencies were calculated for five different cluster models of adsorbed bicarbonate corresponding to different modes of bonding to the surface (see Figure 1). Since both aluminum oxide surfaces and nanoparticulate Fe<sub>2</sub>O<sub>3</sub> showed similar vibrational spectra, calculations were done using the following clusters [M<sub>2</sub>(OH)<sub>4</sub>-( $\mu$ -OH)(H<sub>2</sub>O)<sub>x</sub>(HCO<sub>3</sub><sup>-</sup>)] clusters (where M = Al and  $x = 0$  or 1), as discussed in the Experimental Section.

Cluster model **I** was built to represent the structure proposed in the literature for bicarbonate formation following direct nucleophilic attack of surface hydroxyl groups on gas-phase CO<sub>2</sub>.<sup>18</sup> Cluster model **II** was constructed to represent nucleophilic attack of surface hydroxyl group on neighboring CO<sub>2</sub> preadsorbed on a metal site.<sup>10</sup> Cluster models **III**, **IV**, and **V** represent mono, bidentate, and bridged structures following rearrangement of the initial OH + CO<sub>2</sub> interaction. For example, cluster model **V** is a bridged structure that is feasible as a result of molecular rearrangement of cluster model **II**. There is also various degrees of hydrogen bonding with surface hydroxyl and/or H<sub>2</sub>O groups in these clusters.

In Table 4, calculated vibrational frequencies for the five cluster models are compared to the experimental vibrational frequencies. As discussed in the Experimental Section, calculated vibrational frequencies were scaled by the appropriate scaling factor determined for the bicarbonate ion with the 6-31+G(d) basis set. This scaling factor is 0.9506. It is the scaled frequencies that are given and herein are called the calculated frequencies. Only the frequencies for the characteristic

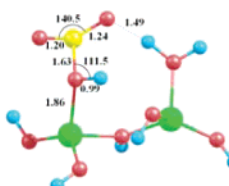
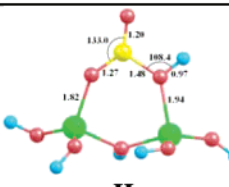
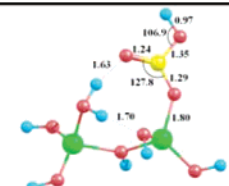
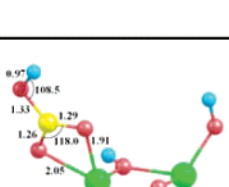
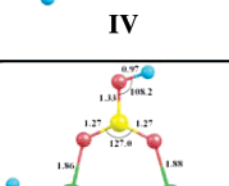
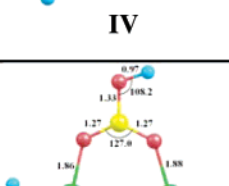
bicarbonate vibrations are given in Table 4. These are the vibrations measured in the spectral region extending from 1200 to 1800 cm<sup>-1</sup>. The O-H stretching mode of adsorbed bicarbonate has also been calculated and, with the exception of cluster model **I**, was found to not differ much for the different structures, whereas the other vibrational modes were found to differ by at least 30 cm<sup>-1</sup> and by as much 270 cm<sup>-1</sup> between the various structures. Therefore, the focus of the discussion below is on the calculated values of the three vibrational modes,  $\nu_2(\text{OCO})_a$ ,  $\nu_3(\text{OCO})_s$ , and  $\delta_4(\text{COH})$ , which are used to compare to the experimental values.

Table 4 gives vibrational frequencies for three of the bicarbonate isotopes for each of the five structures. The three bicarbonate isotopes are HC<sup>16</sup>O<sub>3</sub><sup>-</sup>, from reaction of C<sup>16</sup>O<sub>2</sub> + <sup>16</sup>OH, DC<sup>16</sup>O<sub>3</sub><sup>-</sup>, from reaction of C<sup>16</sup>O<sub>2</sub> + <sup>16</sup>OD, and HC<sup>18</sup>O<sub>3</sub><sup>-</sup>, from reaction of C<sup>18</sup>O<sub>2</sub> + <sup>18</sup>OH. The partially labeled, mixed isotope experiments will be discussed later. The difference between the calculated frequencies,  $\omega$ , and the experimental frequencies,  $\nu$ , for C<sup>16</sup>O<sub>2</sub> adsorption on hydroxylated Al<sub>2</sub>O<sub>3</sub> surfaces, C<sup>16</sup>O<sub>2</sub> adsorption on hydroxylated (OH and OD) nanoparticulate Fe<sub>2</sub>O<sub>3</sub> and C<sup>18</sup>O<sub>2</sub> adsorption on <sup>18</sup>OH-labeled nanoparticulate Fe<sub>2</sub>O<sub>3</sub> are given in the difference column,  $\omega - \nu$ , in Table 4. Since  $\alpha$ -Al<sub>2</sub>O<sub>3</sub> and  $\gamma$ -Al<sub>2</sub>O<sub>3</sub> gave nearly identical infrared spectra, the frequencies in Table 4 are an average of values determined for bicarbonate adsorption on the surface of these two phases. The column labeled vibrational mode and calculated isotope shift,  $\Delta\omega_{\text{iso}}$ , gives the calculated isotope shift observed between the labeled and unlabeled bicarbonate frequencies for the three vibrational modes ( $\Delta\omega_{\text{iso}} = \omega(\text{labeled bicarbonate}) - \omega(\text{unlabeled bicarbonate})$ ). Underneath the calculated values are the experimental isotope shifts,  $\Delta\nu_{\text{iso}}$ . The values for  $\Delta\nu_{\text{iso}}$  are taken from Table 3 for these bicarbonate isotopes adsorbed on nanoparticulate Fe<sub>2</sub>O<sub>3</sub>.

It can be seen in Table 4 that for cluster models **I** and **II**, the calculated frequencies for the  $\nu_2(\text{OCO})_a$  vibration mode are much higher, by over two hundred wavenumbers, than the experimentally measured frequencies. In addition, the  $\nu_3(\text{OCO})_s$  is much lower in frequency compared to the experimental values. The bond length calculated between the carbon atom and the oxygen of the O-H group is 1.63 Å in cluster model **I**. This is unusually long and indicates that adsorbed bicarbonate as shown in structure **I** is quite distorted. In addition, the O-C-O angle in CO<sub>2</sub> is 140.5°, which is significantly larger by ~7–13° than in the other structures. On the basis of the poor agreement between calculated and experimental frequencies, cluster models **I** and **II** are concluded to not represent the structure of bicarbonate on the surface.

There is much better agreement between the experimental and calculated frequencies for cluster models **III**, **IV**, and **V**. To quantify these data, the root-mean-square deviation,  $S$ , for all three vibrational frequencies in all three isotope substitution experiments are given in Table 4 (HC<sup>16</sup>O<sub>3</sub><sup>-</sup>, DC<sup>16</sup>O<sub>3</sub><sup>-</sup>, and

TABLE 4: Vibrational Frequencies ( $\text{cm}^{-1}$ ) of Bicarbonate Ion in  $[\text{M}_2(\text{OH})_4(\mu\text{-OH})(\text{H}_2\text{O})_x(\text{HCO}_3^-)]$  Cluster Models (Where M = Al and  $x = 0$  or 1), Calculated at the DFT/B3LYP/6-31+G(d)//DFT/B3LYP/6-31+G(d) Level of Theory for Several Bicarbonate Isotopes: Comparison to Experimental Values<sup>f</sup>

Cluster Model	Bicarbonate Isotope	Vibrational Mode and Calculated Frequency, $\omega$ , (cm <sup>-1</sup> ) <sup>a</sup>			Vibrational Mode and Difference, $\omega - \nu$ , <sup>b</sup>			Vibrational Mode and Calculated Isotope Shift, $\Delta\omega_{iso}$ , <sup>c</sup> (Experimental Isotope Shift, $\Delta\nu_{iso}$ ) <sup>d</sup>		
		$\nu_2(\text{OCO})_a$	$\nu_3(\text{OCO})_s$	$\delta_4(\text{COH})$	$\nu_2(\text{OCO})_a$	$\nu_3(\text{OCO})_s$	$\delta_4(\text{COH})$	$\nu_2(\text{OCO})_a$	$\nu_3(\text{OCO})_s$	$\delta_4(\text{COH})$
 <b>I</b>	HC <sup>16</sup> O <sub>3</sub> <sup>-</sup>	1877	1220	1165	Al <sub>2</sub> O <sub>3</sub> <sup>e</sup>			n.a. <sup>f</sup>	n.a.	n.a.
				228	-215	-66				
	HC <sup>16</sup> O <sub>3</sub> <sup>-</sup>	1877	1220	1165	nano-Fe <sub>2</sub> O <sub>3</sub>			0	0	0
				255	-190	-55				
	DC <sup>16</sup> O <sub>3</sub> <sup>-</sup>	1875	1214	920	nano-Fe <sub>2</sub> O <sub>3</sub>			-2 (-16)	-6 (0)	-245 (-251)
			269	-196	-49					
 <b>II</b>	HC <sup>16</sup> O <sub>3</sub> <sup>-</sup>	1839	1270	1175	Al <sub>2</sub> O <sub>3</sub>			n.a.	n.a.	n.a.
				190	-165	-56				
	HC <sup>16</sup> O <sub>3</sub> <sup>-</sup>	1839	1270	1175	nano-Fe <sub>2</sub> O <sub>3</sub>			0	0	0
				217	-140	-45				
	DC <sup>16</sup> O <sub>3</sub> <sup>-</sup>	1833	1261	947	nano-Fe <sub>2</sub> O <sub>3</sub>			-6 (-16)	-9 (0)	-228 (-251)
			227	-149	-22					
 <b>III</b>	HC <sup>16</sup> O <sub>3</sub> <sup>-</sup>	1627	1390	1195	Al <sub>2</sub> O <sub>3</sub>			n.a.	n.a.	n.a.
				-22	-45	-36				
	HC <sup>16</sup> O <sub>3</sub> <sup>-</sup>	1627	1390	1195	nano-Fe <sub>2</sub> O <sub>3</sub>			0	0	0
				5	-20	-25				
	DC <sup>16</sup> O <sub>3</sub> <sup>-</sup>	1613	1379	952	nano-Fe <sub>2</sub> O <sub>3</sub>			-14 (-16)	-11 (0)	-243 (-251)
			7	-31	-17					
 <b>IV</b>	HC <sup>16</sup> O <sub>3</sub> <sup>-</sup>	1600	1451	1170	Al <sub>2</sub> O <sub>3</sub>			n.a.	n.a.	n.a.
				-49	16	-61				
	HC <sup>16</sup> O <sub>3</sub> <sup>-</sup>	1600	1451	1170	nano-Fe <sub>2</sub> O <sub>3</sub>			0	0	0
				-22	41	-50				
	DC <sup>16</sup> O <sub>3</sub> <sup>-</sup>	1579	1448	921	nano-Fe <sub>2</sub> O <sub>3</sub>			-21 (-16)	-3 (-0)	-249 (-251)
			-43	38	-48					
 <b>V</b>	HC <sup>16</sup> O <sub>3</sub> <sup>-</sup>	1614	1435	1197	Al <sub>2</sub> O <sub>3</sub>			n.a.	n.a.	n.a.
				-35	0	-34				
	HC <sup>16</sup> O <sub>3</sub> <sup>-</sup>	1614	1435	1197	nano-Fe <sub>2</sub> O <sub>3</sub>			0	0	0
				-8	25	-23				
	DC <sup>16</sup> O <sub>3</sub> <sup>-</sup>	1595	1434	945	nano-Fe <sub>2</sub> O <sub>3</sub>			19 (16)	1 (0)	252 (251)
			-11	24	-24					
 <b>V</b>	HC <sup>18</sup> O <sub>3</sub> <sup>-</sup>	1593	1411	1179	nano-Fe <sub>2</sub> O <sub>3</sub>			21 (23)	24 (22)	18 (15)
				-6	23	-26				

<sup>a</sup> Calculated scaled frequencies (see text for further details). <sup>b</sup> Difference between calculated and experimental frequencies for each mode,  $\omega - \nu$ . <sup>c</sup> Calculated difference in vibrational frequencies between isotopically labeled bicarbonate and unlabeled bicarbonate for each mode,  $\Delta\omega_{\text{iso}}$ . <sup>d</sup> Experimental difference in vibrational frequencies between isotopically labeled bicarbonate and unlabeled bicarbonate for each mode,  $\Delta\nu_{\text{iso}}$ . <sup>e</sup> Average  $\text{Al}_2\text{O}_3$  values given in Table 2. <sup>f</sup> n.a. = not available.

$\text{HC}^{18}\text{O}_3^-$ ), were determined according to eq 2

$$S = \frac{\sqrt{\sum |\omega_i - \nu_i|^2}}{N} \quad (2)$$

where  $\omega_i$  is the calculated vibrational frequency for the  $i$ th vibrational mode,  $\nu_i$  is the experimental vibrational frequency for the  $i$ th vibrational mode, and  $N$  is the number of occurrences

for one structure. The best agreement between calculated and experimental values will result in the smallest value of  $S$ . In the case of iron oxide, the value of  $N$  is nine. For iron oxide, the lowest values of  $S$  were found to be 7 for cluster models **III** and **V**, respectively. The bidentate structure, cluster model **IV**, had a higher  $S$  value of  $14\text{ cm}^{-1}$ . For aluminum oxide,  $N$  is three and  $S$  is lowest for cluster model **V** with a value of 16 compared to 21 and 27 for cluster models **III** and **IV**.



respectively. Further analysis of the calculated and experimental frequencies can be done by looking at the calculated isotope frequency shifts,  $\Delta\omega_{\text{iso}}$ , compared to the experimental isotope shifts,  $\Delta\nu_{\text{iso}}$ , for the bicarbonate vibrational modes given in Table 4.

For the isotope shift frequencies, the focus is on cluster models **III** and **V**, the two cluster models that gave the best fit to the experimental vibrational frequencies. The isotope data show that  $S_{\text{iso}}$ , defined as

$$S_{\text{iso}} = \frac{\sqrt{\sum |\Delta\omega_{\text{iso}} - \Delta\nu_{\text{iso}}|^2}}{N} \quad (3)$$

for the  $\text{DC}^{16}\text{O}_3^-$  isotope, is calculated to be 1.1 for cluster model **V** whereas it is nearly four times higher with a value of 4.0 for cluster model **III**. The  $\text{HC}^{18}\text{O}_3^-$  isotope data is somewhat inconclusive in that similar  $S_{\text{iso}}$  values for both cluster models are found.

Thus, taking all of the data together, the conclusion from our analysis is that cluster model **V**, the bridged structure, is in the greatest agreement with the experimental data. This conclusion comes from both a comparison of the vibrational mode frequencies and the isotope shifts between experimental and calculated values.

Additional calculations were done on other cluster models but poorer agreement between the calculated and experimental frequencies was obtained and they were no longer considered. The cluster models shown in Figure 1 and Table 4 are all neutral clusters. For clusters that contained a water ligand (cluster models **I** and **III**), analogous charged clusters with an OH ligand replacing the water ligand were also energy minimized and the bicarbonate frequencies determined for these charged clusters were calculated. Although the calculated frequencies were slightly different from the ones calculated for the neutral clusters, little change in the conclusions would be made as the calculated frequencies were in poorer agreement with the experimental values and these clusters gave higher values for  $S$  and  $S_{\text{iso}}$ . Another cluster model, a cluster slab that had been previously discussed by Yoon et al. to represent the aluminum oxide lowest energy surface plane ( $\alpha\text{-Al}_2\text{O}_3(0001)$ ),<sup>43</sup> was also calculated for monodentate bicarbonate adsorption (analogous to cluster model **III**). In the cluster slab, there is no opportunity to have hydrogen-bonding interactions between the bicarbonate adsorbate and surface O–H or  $\text{H}_2\text{O}$  groups as there is in cluster model **III**. Without this type of interaction, the agreement between calculated and experimental values is very poor. For example, the scaled calculated value for  $\nu_2(\text{OCO})$  is over  $200\text{ cm}^{-1}$  higher than that found experimentally. Poor agreement is also found for the other vibrational modes, thus a monodentate structure is again discarded from further consideration as the bonding mode of bicarbonate on aluminum and iron oxide surfaces. In addition, Casarin et al. report in a theoretical study using the  $\alpha\text{-Al}_2\text{O}_3(0001)$  slab model that the monodentate bicarbonate structure has a positive  $\Delta H_{\text{ads}}$  when there are no O–H groups or adsorbed  $\text{H}_2\text{O}$  on the surface.<sup>44</sup>

From the above discussion and analysis, we conclude from a comparison of the experimental and calculated frequencies and isotope shifts that cluster model **V** shown in Figure 1 and Table 4 is in greatest agreement. Thus, the bridge structure is proposed to best represent the bonding mode for bicarbonate adsorbed on aluminum and iron oxide surfaces, and other hydroxylated metal oxides that have similar vibrational spectra. To further enhance our understanding of the structure of

adsorbed bicarbonate, mixed isotope substitution calculations were done only on cluster model **V**. Calculated vibrational frequencies and the comparison to experimental frequencies are presented in Table 5.

In the first part of Table 5, mixed isotope bicarbonate clusters with one  $^{18}\text{O}$  substituted oxygen in bicarbonate were calculated in order to compare to the experimental frequencies found for the surface reaction of  $\text{C}^{16}\text{O}_2$  and  $^{18}\text{O}\text{--H}$  on nanoparticulate  $\text{Fe}_2\text{O}_3$  to yield,  $\text{HC}^{18}\text{O}^{16}\text{O}_2^-$  (see Table 3 and Figure 5). In these calculations, the isotope label was moved around to each oxygen in the bicarbonate ion and frequencies were determined for each. In the second part of Table 5, similar calculations of mixed isotope bicarbonate with two oxygens substituted with  $^{18}\text{O}$  were done. These calculations for  $\text{HC}^{16}\text{O}^{18}\text{O}_2^-$  are compared to the experimental frequencies determined for the reaction of  $\text{C}^{18}\text{O}_2$  and  $^{16}\text{O}\text{--H}$  for both nanoparticulate  $\text{Fe}_2\text{O}_3$  and  $\gamma\text{-Al}_2\text{O}_3$ . In the calculation, the two  $^{18}\text{O}$  isotopes were moved around in adsorbed bicarbonate to different sets of oxygen atoms.

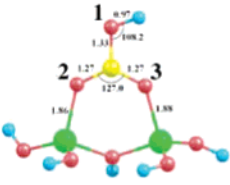
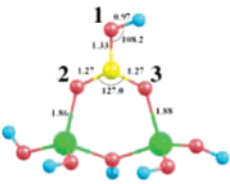
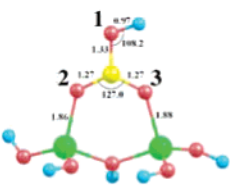
Mixed isotope calculations and experimental data from nanoparticulate  $\text{Fe}_2\text{O}_3$  and  $\gamma\text{-Al}_2\text{O}_3$  are used to determine the best agreement between the experimental vibrational frequencies and the experimental isotope shifts to the calculated values. For the single  $^{18}\text{O}$  label experiment (from the  $\text{C}^{16}\text{O}_2 + ^{18}\text{OH}$  reaction), the agreement is best for  $^{18}\text{O}$  substitution in the 2 and 3 positions, as determined from the minimization of  $S$  and  $S_{\text{iso}}$ , with values of 11 and  $1\text{ cm}^{-1}$ . For the isotope experiments involving two  $^{18}\text{O}$  labels (from the  $\text{C}^{18}\text{O}_2 + ^{16}\text{OH}$  reaction),  $S$  and  $S_{\text{iso}}$  values for both nanoparticulate  $\text{Fe}_2\text{O}_3$  and  $\gamma\text{-Al}_2\text{O}_3$  all fall in the range of 13–15 and 2–3 for all positions. The results of this mixed isotope data are not absolutely conclusive but they suggest that the proton is associated with the O atom in  $\text{CO}_2$  and *not* with the O atom in the O–H moiety it originated from. This surprising result potentially contradicts what has been proposed in the literature as the  $\text{CO}_2$  reaction with surface O–H groups has been described previously as a  $\text{CO}_2$  insertion reaction into the M–OH bond. If this previously proposed mechanism was in fact correct, the proton would *not* be associated with the O atom originating in  $\text{CO}_2$ . This point is elaborated on further in the Discussion section.

**Energetics for the Intramolecular Proton-Transfer Reaction Mechanism.** The analysis of the mixed isotope bicarbonate data above suggests that the proton in the O–H group can migrate to an O atom originating in the  $\text{CO}_2$  reactant molecule. To better understand how this migration or transfer of the proton may proceed, calculations on the intramolecular proton-transfer reaction energetics at 296 K were performed. Calculated energies were done at B3LYP/6-311+G(d,p) and MP2/6-311+G(d,p) levels of theory. The energies determined at the MP2 level are given in parentheses. The calculated values are given in the energy diagram shown in Figure 6. The energies are calculated relative to the initial structure following O–H nucleophilic attack on a neighboring preadsorbed  $\text{CO}_2$  molecule as discussed further in the Discussion (*vide infra*). Following formation of this structure, the proton is transferred from the O–H group to an oxygen atom originating in the  $\text{CO}_2$  reactant molecule. The next step involves recombination of hydrogen atom from the surface O–H to  $\text{CO}_2$  oxygen atoms. The calculated activation energy for the transition state (TS) shown in Figure 6 is 26.24 (25.78) kcal/mol. The product of this proton transfer reaction is energetically favored by  $-14.11$  ( $-13.57$ ) kcal/mol at B3LYP/6-311+G(d,p) and MP2/6-311+G(d,p) levels of theory, with respect to the initial structure.

**Evidence for Isotope Scrambling.** Although the mixed labeled isotope experiments provide useful information, there



**TABLE 5: Vibrational Frequencies ( $\text{cm}^{-1}$ ) of Bicarbonate Ion in  $[\text{M}_2(\text{OH})_4(\mu\text{-OH})(\text{HCO}_3^-)]$  Cluster Model V (where  $\text{M} = \text{Al}$ ), Calculated at DFT/B3LYP/6-31+G(d)//DFT/B3LYP/6-31+G(d) Level of Theory for Several Mixed Isotopes: Comparison to Experimental Values**

$\text{HC}^{18}\text{O}^{16}\text{O}_2^-$ $(^{18}\text{OH} + \text{C}^{16}\text{O}_2)$ <b>nano-<math>\text{Fe}_2\text{O}_3</math></b>	Position of $^{18}\text{O}$ -Label	Vibrational Mode and Calculated Frequency, $\omega$ , ( $\text{cm}^{-1}$ ) <sup>a</sup>			Vibrational Mode and Difference, $\omega - \nu$ <sup>b</sup>			Vibrational Mode and Calculated Isotope Shift, $\Delta\omega_{\text{iso},i}^c$ (Experimental Isotope Shift, $\Delta\nu_{\text{iso}}^d$ ) <sup>μ</sup>		
		$\nu_2(\text{OCO})_a$	$\nu_3(\text{OCO})_b$	$\delta_4(\text{COH})$	$\nu_2(\text{OCO})_a$	$\nu_3(\text{OCO})_b$	$\delta_4(\text{COH})$	$\nu_2(\text{OCO})_a$	$\nu_3(\text{OCO})_b$	$\delta_4(\text{COH})$
 V	1	1613	1430	1187	0	29	-29	-1 (-9)	-5 (-9)	-10 (-4)
	2	1604	1429	1193	-9	28	-23	-10 (-9)	-6 (-9)	-4 (-4)
	3	1607	1424	1192	-6	23	-24	-7 (-9)	-11 (-9)	-5 (-4)
$\text{HC}^{16}\text{O}^{18}\text{O}_2^-$ $(^{16}\text{OH} + \text{C}^{18}\text{O}_2)$ <b>nano-<math>\text{Fe}_2\text{O}_3</math></b>	Position of $^{18}\text{O}$ Substitution	Vibrational Mode and Calculated Frequency, $\omega$ , ( $\text{cm}^{-1}$ ) <sup>a</sup>			Vibrational Mode and Difference, $\omega - \nu$ <sup>b</sup>			Vibrational Mode and Calculated Isotope Shift, $\Delta\omega_{\text{iso},i}^c$ (Experimental Isotope Shift, $\Delta\nu_{\text{iso}}^d$ ) <sup>μ</sup>		
		$\nu_2(\text{OCO})_a$	$\nu_3(\text{OCO})_b$	$\delta_4(\text{COH})$	$\nu_2(\text{OCO})_a$	$\nu_3(\text{OCO})_b$	$\delta_4(\text{COH})$	$\nu_2(\text{OCO})_a$	$\nu_3(\text{OCO})_b$	$\delta_4(\text{COH})$
 V	1,2	1602	1423	1183	-7	34	-26	-12 (-13)	-12 (-21)	-14 (-11)
	2,3	1595	1418	1188	-14	29	-21	-19 (-13)	-17 (-21)	-9 (-11)
	1,3	1606	1417	1184	-3	28	-25	-8 (-13)	-18 (-21)	-13 (-11)
$\text{HC}^{16}\text{O}^{18}\text{O}_2^-$ $(^{16}\text{OH} + \text{C}^{18}\text{O}_2)$ <b><math>\gamma\text{-Al}_2\text{O}_3</math></b>	Position of $^{18}\text{O}$ Substitution	Vibrational Mode and Calculated Frequency, $\omega$ , ( $\text{cm}^{-1}$ ) <sup>a</sup>			Vibrational Mode and Difference, $\omega - \nu$ <sup>b</sup>			Vibrational Mode and Calculated Isotope Shift, $\Delta\omega_{\text{iso},i}^c$ (Experimental Isotope Shift, $\Delta\nu_{\text{iso}}^d$ ) <sup>μ</sup>		
		$\nu_2(\text{OCO})_a$	$\nu_3(\text{OCO})_b$	$\delta_4(\text{COH})$	$\nu_2(\text{OCO})_a$	$\nu_3(\text{OCO})_b$	$\delta_4(\text{COH})$	$\nu_2(\text{OCO})_a$	$\nu_3(\text{OCO})_b$	$\delta_4(\text{COH})$
 V	1,2	1602	1423	1183	-28	7	-32	-12 (-14)	-12 (-22)	-14 (-16)
	2,3	1595	1418	1188	-35	2	-27	-19 (-14)	-17 (-22)	-9 (-16)
	1,3	1606	1417	1184	-24	1	-31	-8 (-14)	-18 (-22)	-13 (-16)

<sup>a</sup> Calculated scaled frequencies (see text for further details). <sup>b</sup> Difference between calculated and experimental frequencies for each mode,  $\omega - \nu$ . <sup>c</sup> Calculated difference in vibrational frequencies between isotopically labeled bicarbonate and unlabeled bicarbonate for each mode,  $\Delta\omega_{\text{iso},i}$ . <sup>d</sup> Experimental difference in vibrational frequencies between isotopically labeled bicarbonate and unlabeled bicarbonate for each mode,  $\Delta\nu_{\text{iso}}$ .

are three pieces of experimental data that show there is some isotope scrambling occurring in the reaction of  $^*\text{OH}$  and  $\text{CO}_2$  over time, where  $^*\text{O}$  represents a different oxygen isotope present in the surface hydroxyl groups than in the  $\text{CO}_2$  reactant molecules. The first suggestion that there is some isotope exchange comes from the FWHM of the absorption bands in the spectra for mixed isotope bicarbonate (see Figure 5). For the mixed isotope experiments, the bands have nearly twice the FWHM compared to the bands in the other experiments. The second more direct measure of exchange is seen in the experiment where  $\text{C}^{18}\text{O}_2$  is adsorbed on nanoparticulate  $\text{Fe}_2\text{O}_3$  that contains  $^{16}\text{OH}$  groups. In the presence of nanoparticulate  $\text{Fe}_2\text{O}_3$ , the gas-phase spectrum of  $\text{C}^{18}\text{O}_2$  changes and incorporates  $^{16}\text{O}$  resulting in a gas-phase spectrum that shifts to higher

frequency as a result of some  $\text{C}^{18}\text{O}^{16}\text{O}$  formation. This scrambling occurs over time scales on the order of 1 h. The third piece of evidence for isotope exchange comes from changes in the O–H stretching region upon adsorption in the mixed isotope experiments. In the experiment where  $\text{C}^{16}\text{O}_2$  is adsorbed on nanoparticulate  $\text{Fe}_2\text{O}_3$  that contains  $^{18}\text{OH}$  surface hydroxyl groups,  $^{16}\text{O}$  incorporation becomes evident as  $^{16}\text{OH}$  is seen to grow in the spectrum after adsorption of  $\text{C}^{16}\text{O}_2$ . The mixed isotope labeling experiments provides additional information about the reaction of  $\text{CO}_2$  with surface O–H groups. The fact that there is scrambling provides an additional indication that the reaction may not just involve a simple  $\text{CO}_2$  insertion reaction into the O–H bond but that proton transfer may occur as well.

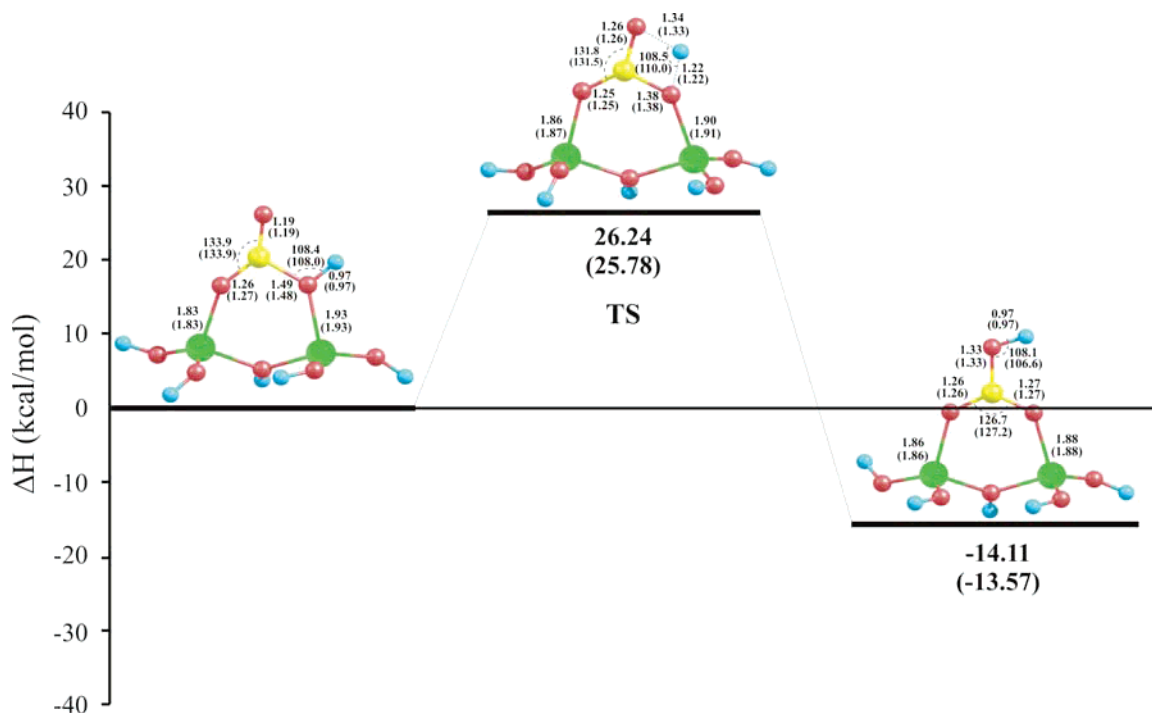


**Figure 6.** Calculated energetics for the intramolecular proton-transfer reaction mechanism. All bond lengths are given in Å and all angles are given in degrees. Optimized structural parameters and relative energies are given at B3LYP/6-311+G(d,p) and MP2/6-311+G(d,p) (in parentheses) levels of theory. See text for further details.

## Discussion

Recent studies have shown that quantum chemical calculations are very useful in understanding the interaction of environmental interfaces, such as oxide surfaces, with atmospheric gases and aqueous pollutants including nitrogen oxides, oxyanions and organic acids.<sup>43–50</sup> In this study, we have used quantum chemical calculations to better understand the adsorption of carbon dioxide on hydroxylated metal oxide surfaces. The combination of FTIR studies of various isotopes of adsorbed bicarbonate and quantum chemical calculations provide information that hitherto had not been available in understanding the surface reaction of gas-phase CO<sub>2</sub> and adsorbed hydroxyl groups to form bicarbonate. Taking these new data into account, along with previous studies on the reaction of CO<sub>2</sub> and surface hydroxyl groups a clearer picture of the reaction chemistry and the adsorbed molecular structure of bicarbonate emerges. As described in detail below, the steps of the reaction include the following: (i) initial CO<sub>2</sub> interaction with surface O–H groups; (ii) nucleophilic attack of adsorbed O–H on CO<sub>2</sub> to form the initial adsorbed bicarbonate structure; (iii) rearrangement of the initial adsorbed bicarbonate structure to form the final bridged bicarbonate structure; (iv) microscopic reversibility that explains the observed isotope scrambling.

Since the reaction to form bicarbonate involves surface hydroxyl groups, it is important to understand what is known about these groups on metal oxide surfaces. For iron oxides, a focus of this study, FTIR spectroscopy has been used to investigate the spectra of various iron oxides in the 3000–4000 cm<sup>−1</sup> range by several investigators.<sup>38,39,51</sup> Up to 11 absorption bands have been observed and assigned to O–H stretching vibrations in various environments.<sup>38</sup> The overall density of OH groups depends on both the crystal structure and on the extent of development of the different crystal faces.<sup>52</sup> For the α-Fe<sub>2</sub>O<sub>3</sub> [100] surface, Barron et al. showed 5.8 singly coordinated OH groups/nm<sup>−2</sup> and 2.9 doubly coordinated OH groups/nm<sup>−2</sup>.<sup>53</sup> The basicity (or acidity) of surface hydroxyl groups will dictate

which groups will be most reactive toward CO<sub>2</sub> molecule. In general, bands assigned to more basic hydroxyl groups appear to be located at higher wavenumbers; the increase in acidity of a hydroxyl group shifts the corresponding bands to a lower wavenumbers.<sup>19,54</sup>

In this study, the decrease in the vibrational bands of O–H groups with frequencies of 3686 and 3664 cm<sup>−1</sup>, shows the involvement of these groups in the formation of adsorbed bicarbonates. These are the O–H groups with the highest frequencies on nanoparticulate Fe<sub>2</sub>O<sub>3</sub> (as shown in ref 42) and therefore are the more basic groups on the surface. Two proposals have been put forth concerning the initial interaction between adsorbed OH groups and CO<sub>2</sub>. Knoezinger et al.<sup>55</sup> proposed the formation of surface bicarbonate involving the reaction of preadsorbed CO<sub>2</sub> on acidic sites in close proximity to basic O–H groups (Langmuir–Hinshelwood type mechanism). Experimental evidence of the presence of an activated preadsorbed species has been found.<sup>20,56</sup> Ramis et al. observed several adsorbed CO<sub>2</sub> species on several metal oxides at temperatures between 173 and 273 K including an activated or bent CO<sub>2</sub> species that were characterized by absorption bands in the spectral regions extending from 1650 to 1900 cm<sup>−1</sup> and 1150 to 1320 cm<sup>−1</sup>, respectively.<sup>20</sup> In contrast, others have proposed nucleophilic attack on CO<sub>2</sub> when it is in close proximity but not adsorbed on the surface (which resembles more of an Eley–Rideal type mechanism).<sup>18,57–59</sup>

The experimental data shown here suggests in fact that the Langmuir–Hinshelwood type mechanism involving two neighboring sites with adsorbed CO<sub>2</sub> and adsorbed OH may best explain the formation of the final bridged structure, which also involves two neighboring sites. The proposed first step then is for CO<sub>2</sub> to adsorb on a site next to adsorbed OH or for adsorbed OH in a bridged configuration to accommodate the gas-phase CO<sub>2</sub> molecule. This accommodation shown in the mechanism shown in the first step of Figure 7a also explains the involvement of bridged O–H groups in the reaction. The next step in the

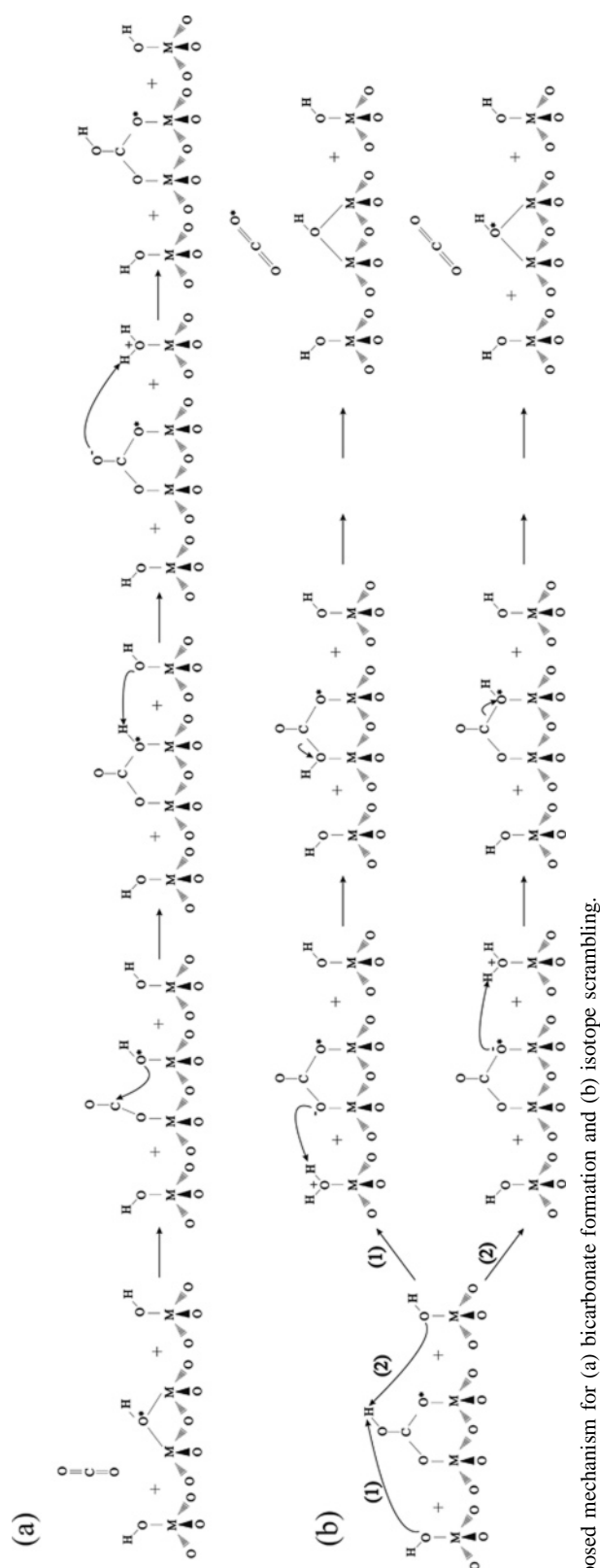


**Figure 7.** Proposed mechanism for (a) bicarbonate formation and (b) isotope scrambling.

reaction involves nucleophilic attack of adsorbed OH on the activated CO<sub>2</sub> molecule, as shown in Figure 7a. The initial bicarbonate structure shown in Figure 7a is analogous to the bicarbonate structure shown in cluster model II.

As determined from the analysis of the vibrational frequencies in the previous sections, this is not the final structure. The final structure must involve molecular rearrangement. The mixed isotope experiments suggest that the mechanism for molecular rearrangement may involve proton transfer so that the original O—H bond is broken. Although the rearrangement to form the final bicarbonate structure is calculated to be thermodynamically favored, there is a high barrier for intramolecular proton-transfer calculated to be 25.58 and 25.05 kcal mol<sup>-1</sup> at the B3LYP/6-311+G(d,p) and MP2/6-311+G(d,p) levels of theory. Thus, the intramolecular proton transfer mechanism is not a likely pathway.

In general, it is known that intermolecular proton transfer is a typically lower energy pathway.<sup>60,61</sup> On an extended surface, other surface groups such as carbonate and OH groups may provide an intermolecular pathway. The mechanism shown in Figure 7a shows the potential participation of other adsorbed OH groups in the reaction and how they may be involved in proton transfer. Carbonate groups adsorbed on the surface may also be involved (not shown). The intermolecular proton transfer leads to the final bicarbonate structure. The bridged structure determined for bicarbonate on oxide surfaces agrees well with a recent electrochemical study by Berna et al.<sup>61</sup> who showed through reflectance absorption infrared spectroscopy combined with quantum chemical calculations that bicarbonate adsorption on Pt(111) and Pd/Pt(111) formed what they called a “short-bridge bidentate” configuration for potentials below 0.65 V.

Furthermore, it is easy to see how isotope scrambling may readily occur in this mechanism. Figure 7a shows the reaction between \*OH and CO<sub>2</sub>, where \*O represent a different oxygen isotope present in the surface hydroxyl groups than in the CO<sub>2</sub> reactant molecules. Figure 7b shows two pathways in which adsorbed bicarbonate reversibly forms carbon dioxide in the gas phase. In one pathway, CO<sub>2</sub> is formed whereas in the other pathway CO\*O forms. The proposed mechanism then also explains the isotope scrambling that is observed.

Thus, some of the key aspects of the proposed mechanism shown in Figure 7 are that (i) CO<sub>2</sub> molecules are preadsorbed and activated prior to partial donation of the lone pair from HOMO in the surface hydroxyl group oxygen to form a new C—O bond, (ii) neighboring groups, e.g., OH groups, are involved in proton transfer, (iii) the proposed mechanism explains the bridged bicarbonate structure on the surface that is determined from the comparison between the experimental and calculated vibrational data for all bicarbonate isotopes including mixed isotopes, and (iv) the proposed mechanism explains the isotope scrambling seen in the gas phase.

It has also been calculated that CO<sub>2</sub> insertion mechanism is a very low energy pathway.<sup>45,58,59</sup> This process can also occur but there may be intermolecular proton transfer as well following the insertion mechanism. Further scrambling can occur as the gas-phase CO<sub>2</sub> becomes isotopically impure through adsorption-reaction-desorption equilibria.

## Conclusions

Transmission FTIR spectroscopy combined with isotope labeling experiments are used to gain a better understanding of the adsorption and reaction of CO<sub>2</sub> with hydroxylated metal oxide surfaces, in particular iron and aluminum oxides. In this study, the discussion is focused on the adsorbed bicarbonate



product, the product whose absorption bands often dominate the infrared spectrum in the presence of gas-phase CO<sub>2</sub>. It is shown here that adsorbed bicarbonate forms a bridged structure on the surface. The formation of the bridged bicarbonate structure is proposed to occur through a nucleophilic attack of adsorbed CO<sub>2</sub> by surface O–H groups followed by rearrangement on the surface. An intermolecular proton-transfer involving neighboring hydroxyl and/or carbonate groups is proposed to occur on the surface to explain the vibrational data. The proposed mechanism for bicarbonate formation explains the isotope scrambling that is observed in the mixed labeled experiments. The results presented here provide a detailed look at the interaction between carbon dioxide, an important atmospheric gas, and oxide interfaces.

**Acknowledgment.** This material is based upon work supported by the National Science Foundation under Grant No. CHE-0503854 (V.H.G.) and MCB-0209941 (J.H.J.). Any opinions, findings, and conclusions or recommendations expressed in this material are those of the author(s) and do not necessarily reflect the views of the National Science Foundation. The authors gratefully acknowledge this support. The authors also thank Jennifer Schuttlefield for her contributions to the mixed isotope experiments, Dr. David Cwiertny for Mossbauer spectroscopy of nanoparticulate Fe<sub>2</sub>O<sub>3</sub> and Prof. Mark Arnold for helpful discussions.

**Supporting Information Available:** Table of calculated vibrational frequencies and structures of I–V. This material is available free of charge via the Internet at <http://pubs.acs.org>.

## References and Notes

- Weissmehl, K.; Arpe, H. *J. Industrial Organic Chemistry. Important Initial and Intermediate Products*; Verlag Chemie: Weinheim, Germany, 1976.
- Freund, H. J.; Roberts, M. W. *Surf. Sci. Rep.* **1996**, 25, 227.
- Henrich, V. E.; Cox, P. A. *The Surface Science of Metal Oxides*; Cambridge University Press: Cambridge, U.K., 1994.
- Davydov, A. A. *Infrared Spectroscopy of Adsorbed Species on the Surface of Transition Metal Oxides*; Wiley: New York, 190.
- Brown, G. E., Jr.; Henrich, V. E.; Casey, W. H.; Clark, D. L.; Eggleston, C.; Felmy, A.; Goodman, D. W.; Graetzel, M.; Maciel, G.; McCarthy, M. I.; Nealson, K. H.; Sverjensky, D. A.; Toney, M. F.; Zachara, J. M. *Chem. Rev.* **1999**, 99, 77.
- Stumm, W. *Chemistry of the Solid-Water Interface: Processes at the Mineral–Water and Particle–Water Interface in Natural Systems*; Wiley: New York, 1992.
- Al-Abadleh, H. A.; Grassian, V. H. *Surf. Sci. Rep.* **2003**, 52, 63.
- Finlayson-Pitts, B. J.; Wingen, L. M.; Sumner, A. L.; Syomin, D.; Ramazan, K. A. *Phys. Chem. Chem. Phys.* **2003**, 5, 223.
- Martin, J. H.; Fitzwater, S. E. *Nature (London)* **1988**, 331, 341.
- Zhu, X. R.; Prospero, J. M.; Millero, F. J. *J. Geophys. Res.* **1997**, 102, 21297.
- Jickells, T. D.; An, Z. S.; Andersen, K. K.; Baker, A. R.; Bergametti, G.; Brooks, N.; Cao, J. J.; Boyd, P. W.; Duce, R. A.; Hunter, K. A.; Kawahata, H.; Kubilay, N.; LaRoche, J.; Liss, P. S.; Mahowald, N.; Prospero, J. M.; Ridgwell, A. J.; Tegen, I.; Torres, R. *Science* **2005**, 308, 67.
- Meskhidze, N.; Chameides, W. L.; Nenes, A.; Chen, G. *Geophys. Res. Lett.* **2003**, 30, 2085, doi:10.1029/2003GL018036.
- Busca, G.; Lorenzelli, V. *Mater. Chem.* **1982**, 7, 89.
- Krylov, O. V.; Kiselev, V. F. *Adsorption and Catalysis on Transition Metals and Their Oxides*; Springer Series in Surface Sciences; Ertl, G., Gomer, R., Eds.; Springer-Verlag: Berlin, 1989; Vol. 9.
- Morterra, C.; Zecchina, A.; Coluccia, S.; Chiorino, A. *J. Chem. Soc., Faraday Trans. 1* **1977**, 73, 1544.
- Ferretto, L.; Glisenti, A. *J. Mol. Catal. A: Chem.* **2002**, 187, 119.
- Parkyn, N. D. *J. Phys. Chem.* **1971**, 75, 526.
- Hoggan, P. E.; Bensitel, M.; Lavalley, J. C. *J. Mol. Struct.* **1994**, 320, 49.
- Turek, A. M.; Wachs, I. E.; DeCanio, E. *J. Phys. Chem.* **1992**, 96, 5000.
- Ramis, G.; Busca, G.; Lorenzelli, V. *Mater. Chem. Phys.* **1991**, 29, 425.
- Brintzinger, H.; Hester, R. E. *Inorg. Chem.* **1966**, 5, 980.
- Taravel, B.; Chauvet, G.; Delorme, P.; Lorenzelli, V. *J. Mol. Struct.* **1972**, 13, 283.
- Auroux, A.; Gervasini, A. *J. Phys. Chem.* **1990**, 94, 6371.
- Rethwisch, D. G.; Dumesic, J. A. *Langmuir* **1986**, 2, 73.
- Jung, T. J.; Bell, A. T. *J. Catal.* **2001**, 204, 339.
- Novak, A.; Saumagne, P.; Bok, L. D. C. *J. Chim. Phys. Physico-Chim. Biol.* **1963**, 60, 1385.
- Nakamoto, K.; Sarma, Y. A.; Ogoshi, H. *J. Chem. Phys.* **1965**, 43, 1177.
- Bernitt, D. L.; Hartman, K. O.; Hisatsune, I. C. *J. Chem. Phys.* **1965**, 42, 3553.
- Maguire, P. M.; Rubalcava, H. E. *Inorg. Chem.* **1969**, 8, 246.
- Yoshida, T.; Thorn, D. L.; Okano, T.; Ibers, J. A.; Otsuka, S. *J. Am. Chem. Soc.* **1979**, 101, 4212.
- Flynn, B. R.; Vaska, L. *J. Am. Chem. Soc.* **1973**, 95, 5081.
- Li, G. H.; Xu, M.; Grassian, V. H.; Larsen, S. C. *J. Mol. Catal. A* **2003**, 194, 169.
- Grassian, V. H. *J. Phys. Chem. A* **2002**, 106, 860.
- Kong, J.; White, C. A.; Krylov, A. I.; Sherrill, D.; Adamson, R. D.; Furlani, T. R.; Lee, M. S.; Lee, A. M.; Gwaltney, S. R.; Adams, T. R.; Ochsenfeld, C.; Gilbert, A. T. B.; Kedziora, G. S.; Rassolov, V. A.; Maurice, D. R.; Nair, N.; Shao, Y.; Besley, N. A.; Maslen, P. E.; Dombroski, J. P.; Daschel, H.; Zhang, W.; Korambath, P. P.; Baker, J.; Byrd, E. F. C.; Van Voorhis, T.; Oumi, M.; Hirata, S.; Hsu, C.-P.; Ishikawa, N.; Florian, J.; Warshel, A.; Johnson, B. G.; Gill, P. M. W.; Head-Gordon, M.; Pople, J. A. *J. Comput. Chem.* **2000**, 21, 1532.
- <http://www.chemcraftprog.com>.
- See <http://srdata.nist.gov/cccbdb/> (NIST), Release 11, May 2005.
- Wong, M. W. *Chem. Phys. Lett.* **1996**, 256, 391.
- Rochester, C. H.; Topham, S. A. *J. Chem. Soc., Faraday Trans. 1* **1979**, 75, 1073.
- Busca, G.; Lorenzelli, V. *Mater. Chem.* **1980**, 5, 213.
- Magnacca, G.; Cerrato, G.; Morterra, C.; Signoretto, M.; Somma, F.; Pinna, F. *Chem. Mater.* **2003**, 15, 675.
- Surface hydroxyl groups were exchanged with either 10 Torr of D<sub>2</sub>O (at T = 295 K) or H<sub>2</sub><sup>18</sup>O (at T = 373 K) to yield surface, DO–Fe or H<sup>18</sup>O–Fe, respectively. The exchange was done multiple times and was monitored by FTIR spectroscopy. See ref 42 for further details.
- Baltrusaitis, J.; Grassian, V. H. *J. Phys. Chem. B* **2005**, 109, 12227.
- Yoon, T. H.; Johnson, S. B.; Musgrave, C. B.; Brown, G. E., Jr. *Geochim. Cosmochim. Acta* **2004**, 68, 4505.
- Casarin, M.; Falcomer, D.; Vittadini, A. *Surf. Sci.* **2004**, 566–568, 890.
- Casarin, M.; Falcomer, D.; Gilsenti, A.; Vittadini, A. *Inorg. Chem.* **2003**, 42, 436.
- Usher, C. R.; Paul, K. W.; Narayansamy, J.; Kubicki, J. D.; Sparks, D. L.; Schoonen, M. A. A.; Strongin, D. R. *Environ. Sci. Technol.* **2005**, 39, 7576.
- Thompson, K. C.; Margey, P. *Phys. Chem. Chem. Phys.* **2003**, 5, 2970.
- Kwon, K. D.; Kubicki, J. D. *Langmuir* **2004**, 20, 9249.
- Paul, R. W.; Borda, M. J.; Kubicki, J. D.; Sparks, D. L. *Langmuir* **2005**, 21, 11071.
- Ishikawa, T.; Cai, W. Y.; Kandori, K. *Langmuir* **1993**, 9, 1125.
- Cornell, R. M.; Schwertmann, U., Eds.; *The Iron Oxides: Structure, Properties, Reactions, Occurrence and Uses*; VCH: Weinheim, Germany, 1996.
- Barron, V.; Torrent, J. *J. Colloid Interface Sci.* **1996**, 177, 407.
- Anderson, P. J.; Horlock, R. F.; Oliver, J. F. *Trans. Faraday Soc.* **1965**, 61, 2754.
- Knoezinger, H. *Adv. Catal.* **1976**, 25, 184.
- Morterra, C.; Orio, L. *Mater. Chem. Phys.* **1990**, 24, 247.
- Tsyganenko, A. A.; Trusov, E. A. *Zh. Fiz. Khim.* **1985**, 59, 2602.
- Lamotte, J.; Saur, O.; Lavalley, J. C.; Busca, G.; Rossi, P. F.; Lorenzelli, V. *J. Chem. Soc., Faraday Trans. 1* **1986**, 82, 3019.
- Markovits, A.; Fahmi, A.; Minot, C. *THEOCHEM* **1996**, 371, 219.
- Jensen, J. H.; Baldrige, K. K.; Gordon, M. S. *J. Phys. Chem.* **1992**, 96, 8340.
- Gordon, M. S. *J. Phys. Chem.* **1996**, 100, 3974.
- Berna, A.; Rodes, A.; Feliu, J. M.; Illas, F.; Gil, A.; Clotet, A.; Ricart, J. M. *J. Phys. Chem. B* **2004**, 108, 17928.